1851. Development and verification of time-dependent bounding surface model under metro dynamic loads

Junhui Luo[1], Linchang Miao[2], Renjue Li[3], Wenbo Shi[4], Yinan Chen[5], Bo Yan[6]
[1, 2, 4, 5]Institute of Geotechnical Engineering of Southeast University, Nanjing 210096, China
[3]Changzhou Institute of Technology, Changzhou 213002, China
[6]Research and Design Institute of Urban Rail Transit of Jiangsu Province, Nanjing 210008, China
[2]Corresponding author
E-mail: [1]*juluo85@hotmail.com*, [2]*lc.miao@seu.edu.cn*, [3]*lirenjue@vip.qq.com*, [4]*shwanbe@163.com*,
[5]*chen-yinan_d@163.com*, [6]*nrts_yb@163.com*

Abstract. To study the dynamic characteristics of soft soil foundation under the long-term metro dynamic loads, modified model based on the bounding surface model was presented. The Mesri creep formula was introduced into the bounding surface model, then it could not only consider the effects of time but also could describe the soil's arbitrary shear stress levels. The modified bounding surface model was derived using the Newton-Raphson method and the secondary development of the model was conducted. Meanwhile, in order to verify the model, the dynamic triaxial tests of the soft soil were conducted by GDS dynamic triaxial equipment and the metro dynamic loads were simulated during dynamic triaxial tests. Then, the numerical simulation of modified bounding surface model was carried out for soft soil and the numerical results were compared with the test results. The results show that the time-dependent bounding surface model provides a more accurate calculation for the dynamic strain, and establishes a theoretical foundation for predicting the settlement of the soft soil.

Keywords: metro dynamic loads, dynamic characteristics, vibration, soft clay, time-dependent.

1. Introduction

Bjerrum was the first scholar to research on the soft soil and proposed the concept of total strain decomposition [1]. It was found that the soft soil area has high compression, high water content, low permeability, creep engineering properties. The soft soil foundation will produce greater amounts of long-term settlement in the subway given the vibration occurring as a result of the moving loads [2]. In order to more accurately calculate the settlement of soft soil during subway vibration operation, it is necessary to establish a dynamic constitutive model consideration time effects under dynamic loads [3].

Current plastic models typically employ the bounding surface model to study dynamic soil characteristics. Dafalias proposed the mathematic expression of the bounding surface model [4-6]. Compared with the cam-clay model, the bounding surface model could better describe the plastic hysteresis characteristics of the soil in calculations of the dynamic strain-stress soil relations under the dynamic loads [7, 8]; consequently, it was often used to analyze dynamic problem [9, 10].

The creep empirical model has two types: Singh-Mitchell and the Mesri creep model. The former model can only be calculated for the 20 %-80 % range of the shear stress level and Mesri model improved this problem [11-13]. Then numerous studies on the creep empirical model under dynamic loads have been carried out [14, 15]. However, these studies are not suitable for the numerical simulation analysis of soil settlement under dynamic loads.

Along with these problems, studying the dynamic characteristics and settlement of soft soil foundation under long-term vibration, this paper introduces the Mesri creep model into the boundary surface model. A time-dependent boundary surface model was developed to describe soil creep for arbitrary shear stress levels. Meanwhile, in order to verify the model, the dynamic triaxial tests of the soft soil were conducted and the subway metro dynamic load modes was simulated during the dynamic triaxial tests. Then, the modified bounding surface model was used to simulate for soft soil and the numerical results were compared with the test results. The study

of soft soil characteristics under metro dynamic loads provides a theoretical foundation for subsidence prediction.

2. Establishment of the time-dependent bounding surface model under dynamic loads

The modified bounding surface model was derived on the basis of the rheological model, the yield criterion, hardening law and flow rule. Based on the incremental theory [16, 17], the total strain $d\varepsilon_{ij}$ is divided into the sum of three partial strain increments:

$$d\varepsilon_{ij} = d\varepsilon_{ij}^e + d\varepsilon_{ij}^p + d\varepsilon_{ij}^t, \tag{1}$$

where $d\varepsilon_{ij}^e$ is the elastic strain increment; $d\varepsilon_{ij}^p$ is the plastic strain increment; and $d\varepsilon_{ij}^t$ is the creep increment.

2.1. Creep increment

The creep increment is divided into volumetric creep and deviatoric stress creep:

$$d\varepsilon_{ij}^t = \frac{d\varepsilon_v^t}{3} + d\varepsilon_s^t \frac{de_{ij}}{q}, \tag{2}$$

where $d\varepsilon_v^t$ is volumetric creep increment; $d\varepsilon_s^t$ is the deviatoric stress creep; and de_{ij} is the partial strain.

2.1.1. Deviatoric stress creep

Deviatoric stress creep is based on the Mesri creep model. The Mesri model was created as an improvement on the classic Singh-Mitchell creep model. The Singh-Mitchell creep model can only describe 20 %-80 % of soil creep properties for shear stress levels, and when the shear stress level is equal to zero, the strain calculation results are less than zero. For this problem, the Mesri model had been improved to calculate the soil creep under arbitrary shear stress levels.

According to the Singh-Mitchell creep formula:

$$d\varepsilon_s^t = Ae^{\overline{\alpha}\overline{D}} \left[\frac{(t)_i}{t} \right]^m dt, \tag{3}$$

where A, $\overline{\alpha}$, and m are the testing parameters; $(t)_i$ is the elapse time, usually set to unity; $\overline{D} = (\sigma_1 - \sigma_3)/(\sigma_1 - \sigma_3)_f$ is the shear stress level; and $1/2 (\sigma_1 - \sigma_3)_f = S_u$ is the undrained shear strength.

Under dynamic loads, an equivalent linear model by Hardin-Drnevich [18, 19] has been proposed:

$$(\sigma_1 - \sigma_3)_d = \frac{\varepsilon_d}{a + b\varepsilon_d}, \tag{4}$$

where $(\sigma_1 - \sigma_3)_d$ is dynamic deviatoric stress; a and b are the testing parameters; and ε_d is dynamic strain. E_d is initial dynamic modulus and $(\sigma_1 - \sigma_3)_{ult}$ is the final principal stress difference:

$$E_d = \frac{d(\sigma_1 - \sigma_3)_d}{d\varepsilon_d}\bigg|_{\varepsilon=0} = \frac{1}{a}, \quad (\sigma_1 - \sigma_3)_{ult} = \lim_{\varepsilon \to \infty} \frac{\varepsilon_d}{a + b\varepsilon_d} = \frac{1}{b},$$

and $R_f = (\sigma_1 - \sigma_3)_f / (\sigma_1 - \sigma_3)_{ult}$ is damage ratio.

Eq. (4) can therefore be achieved:

$$\varepsilon = \frac{2}{(E_d/S_u)} \frac{\overline{D}}{1 - (R_f)\overline{D}} \tag{5}$$

Via combining Eq. (3) with Eq. (5) it obtain:

$$d\varepsilon_s^t = \frac{2}{(E_d/S_u)} \frac{\overline{D}}{1 - (R_f)\overline{D}} \left[\frac{(t)_i}{t}\right]^m dt. \tag{6}$$

2.1.2. Volumetric creep

Taylor's derived creep incremental volume [20] is as follows:

$$d\varepsilon_v^t = \frac{C_\alpha}{2.3(1 + e_0)t_v}, \tag{7}$$

where C_α is the secondary consolidation coefficient; $t_v = \exp(e_2 - e_1/\psi)$; $\psi = C_\alpha/2.3$; e_0 is the initial void ratio; and e_1 is the existing void ratio. The expression of the formula is $e_1 = e_a - (\lambda - \kappa)\ln p_c - \kappa\ln p$. λ and κ are the cam-clay model parameters; p_c is the law of hardening parameters and also is the preconsolidation pressure, equal to the yield surface and the p axis intersection; e_a is the void ratio in an isotropic consolidation curve corresponding to $p_c = 1$ [21]; and e_2 is void ratio corresponding in a state of normal consolidation under the stress state. Thus, the expression of the formula is $e_2 = e_a - (\lambda - \kappa)\ln p_0 - \kappa\ln p$. p_0 is the equivalent consolidation pressure, and the expression for the formula is:

$$p_0 = p + \frac{q^2}{M^2 p}. \tag{8}$$

2.2. The plastic strain increment

2.2.1. The yield surface equation

Based on bounding surface model, modified cam-clay yield surface model proposed by Manzari was chosen; Because of the hardening parameter p_c improved functionality with consideration to the time factor, and yield surface changes over time in Fig. 1. Use the tensor as follows:

$$F = \overline{s}_{ij}\overline{s}_{ij} - \frac{2}{3}M^2\overline{p}(p_c - \overline{p}), \tag{9}$$

where $s_{ij} = \sigma_{ij} - p\delta_{ij}$; $p = \sigma_{ii}$; δ_{ij} is the Kronecker delta; $\overline{s}_{ij}$ and $\overline{p}$ are image points on the boundary corresponding to real stress points; M is the critical state line slope; p_c is the intersection of the yield surface and the p axis, which is the size of the boundary and will change over time; and $\overline{\sigma}_{ij} = b\sigma_{ij}$, $b \geq 1$ is the ratio of the mapping points to the actual stress on the yield surface.

2.2.2. Hardening rule

According to the theory of critical state soil mechanics, the isotropic consolidation test and rebound test can obtain a hardening rule:

$$\frac{\partial p_c}{\partial \varepsilon_v^p} = \frac{1+e}{\lambda - \kappa} p_c. \tag{10}$$

Based on the literature [22] and according to Fig. 2, the improved hardening parameter for considering time effect is as follows:

$$p_c = p_c(\varepsilon_v^p, t_v). \tag{11}$$

Considering the time factor, Fig. 2 can be used to derive a void ratio increment as follows:

$$-\Delta e = \psi \ln\left(1 + \frac{\Delta t_v}{t_v}\right) = (\lambda - \kappa)\ln\left(1 + \frac{\Delta p_c}{p_c}\right). \tag{12}$$

Eq. (12) can be reduced to:

$$\frac{\Delta p_c}{p_c} = \left(1 + \frac{\Delta t_v}{t_v}\right)^{\frac{\psi}{\lambda - \kappa}} - 1. \tag{13}$$
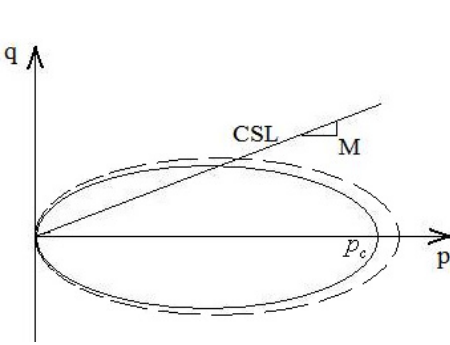
Fig. 1. Schematic view of the yield surfaces in q-p stress space
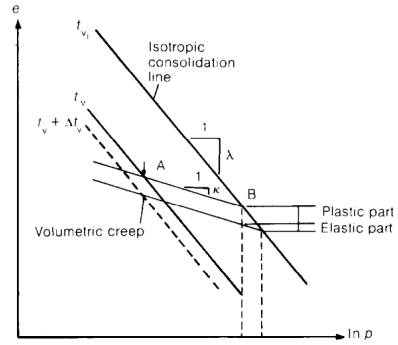
Fig. 2. Incorporation of time factor in isotropic consolidation and rebound test parameters

Taking the Taylor series expansion for Eq. (13), it obtains:

$$\frac{\partial p_c}{\partial t_v} = \frac{\psi}{\lambda - \kappa} \frac{p_c}{t_v}. \tag{14}$$

Applying the total differential definition for Eq. (14) and combining Eqs. (10) and (14), it can derive the following:

$$dp_c = \left.\frac{\partial p_c}{\partial \varepsilon_v^p}\right|_{t_v} d\varepsilon_v^p + \left.\frac{\partial p_c}{\partial t_v}\right|_{\varepsilon_v^p} dt_v = \frac{1+e}{\lambda - \kappa} p_c d\varepsilon_v^p + \frac{\psi}{\lambda - \kappa} \frac{p_c}{t_v} dt. \tag{15}$$

2.2.3. Flow rule

According to the theory of plasticity, plastic deformation $d\varepsilon_{ij}^p$ is divided into plastic volume strain $d\varepsilon_v^p$ and deviatoric strain de_{ij}^p:

$$d\varepsilon_v^p = \Lambda \frac{\partial F}{\partial \bar{p}} = \Lambda \frac{4}{3} M^2 \left(\bar{p} - \frac{1}{2} p_c\right), \tag{16}$$

$$de_{ij}^p = \Lambda \frac{\partial F}{\partial \overline{s}_{ij}} = \Lambda 2 \overline{s}_{ij}, \tag{17}$$

where:

$$\Lambda = \frac{1}{\overline{K}_p}\left[\frac{\partial F}{\partial \overline{\sigma}_{kl}}d\overline{\sigma}_{kl}\right] = \frac{1}{K_p}\left[\frac{\partial F}{\partial \overline{\sigma}_{kl}}d\sigma_{kl}\right],$$

and $\overline{K}_p$ is the point of reference for the bounding surface plastic modulus; and K_p is the current stress point of the plastic modulus. Two of these plastic modulus values use the recommendation of Manzaei [23], as shown below:

$$K_p = \overline{K}_p + H_0 \frac{16M^4 v}{9(\lambda - \kappa)}\overline{p}^3\left(\frac{b-1}{b}\right) = \frac{8M^4 v}{9(\lambda - \kappa)}p_c\left(\overline{p} - \frac{p_c}{2}\right)\overline{p} + H_0\frac{16M^4 v}{9(\lambda - \kappa)}\overline{p}^3\left(\frac{b-1}{b}\right). \tag{18}$$

2.3. The elastic part

The function is:

$$d\varepsilon_v^e = \frac{dp}{K}, \quad de_{ij}^p = \frac{ds_{ij}}{2G}, \tag{19}$$

where $d\varepsilon_v^e$ is the elastic volumetric strain increment, and according to Hooke's law:

$$K = \frac{vp}{\kappa}, \quad G = \frac{3K(1 - 2\mu)}{2(1 + \mu)}.$$

2.4. Implicit integration of the model

Based on the concept of the implicit backward Euler method [24], calculation steps can be divided into two steps: (1) the elastic response and (2) viscoplastic correction. According to Eq. (1)-(19) and ref. [25], the derivation formulas can be obtained, as detailed in the appendix A.

The Newton-Raphson algorithm was used to solve the equation sets (R_i) also in the appendix A [26]. The iterations were stopped when the iterative error $R_i^{(k)}$ was less than the allowable values. When k iteration is used to calculate $\partial R_i^{(k)}/\partial(X)_{n+1}$ and $\partial R_i^{(k)}/\partial(X)_{n+1} \cdot \delta(X)_{n+1} = -R_i$, then the tangent modulus is obtained at the same time (see appendix A).

3. The parameters of model

The time-dependent bounding surface model combines the advantages of the Mesri creep model, critical state soil mechanics theory, and the boundary surface model theory [27]. Meanwhile, the parameters are concise and easy to determine. This work focuses on the study of soft soil, and the following parameter influence analysis can be obtained via laboratory test data.

3.1. Creep parameters

Given Eq. (4), it can obtain a linear relation between $1/E_d$ and ε_d, thereby obtaining parameters a and b. It then derived E_d/S_u and R_f [28, 29]. S_u was obtained using indoor unconfined compressive strength tests. As shown in Fig. 3, the $\sigma_d \sim \varepsilon_d$ hyperbolic equation has been converted into a linear equation. This was calculated using the least square method results in the linear intercept a and slope b. The E_d/S_u were obtained using a and S_u. The analysis

parameters under the condition of differing dynamic amplitudes are shown in Fig. 4.

Analysis parameters (R_f) under the condition of different dynamic amplitudes are shown in Fig. 5. Using Eq. (9) to calculate the parameter m from dynamic strain vs. time relationship curve in Fig. 6.
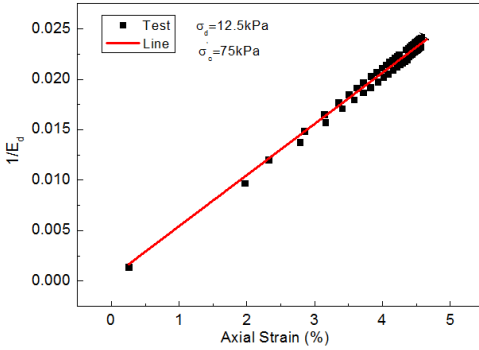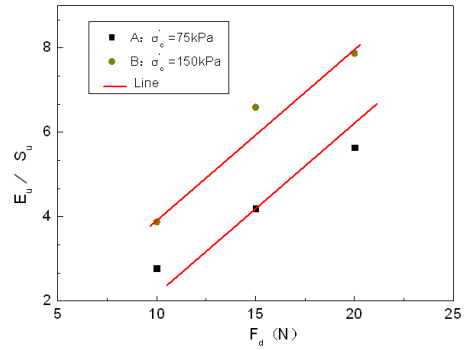

Fig. 3. $1/E_d \sim \varepsilon_d$ relationship diagram
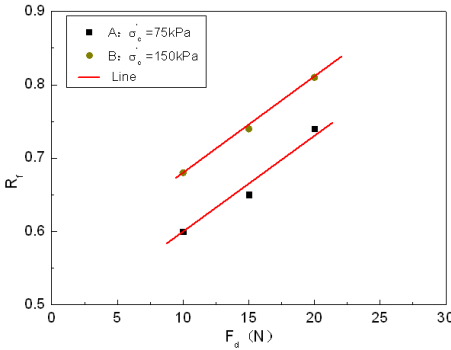

Fig. 4. $E_d/S_u \sim F_d$ relationship diagram
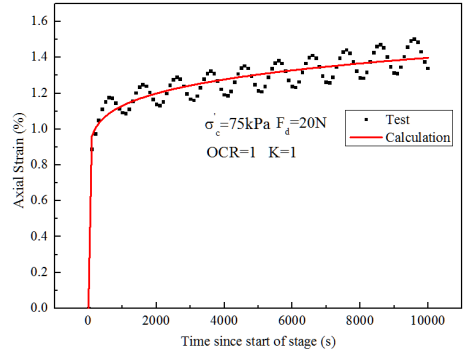

Fig. 5. $R_f \sim F_d$ relationship diagram

Fig. 6. Strain vs. time relationship diagram
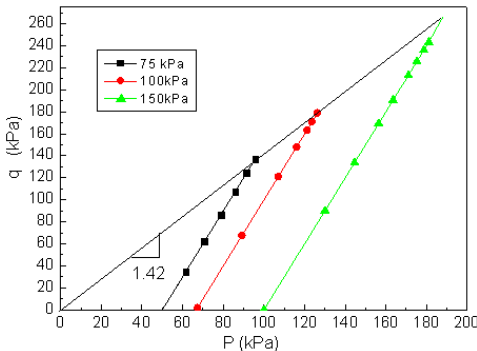
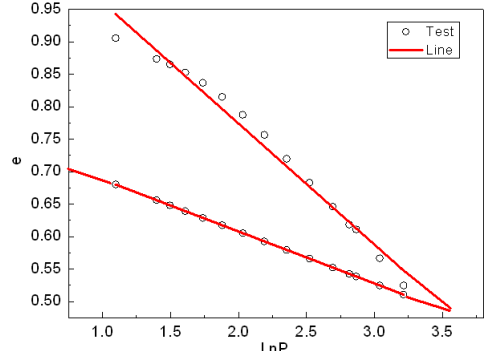**Fig. 7.** The $q \sim p$ relationship in consolidated drained conditions

Fig. 8. The isotropic consolidation and rebound test

3.2. Critical state model parameters

Based on critical state soil mechanics theory, the critical stress ratio M in Fig. 7 can be obtained through the consolidated drained test; q represents the effective deviatoric stress; p is the effective confining pressure. The isotropic consolidation and rebound experiments were used to obtain the parameters λ and κ.

3.3. Plastic modulus parameter H_0

Parameter H_0 affects the form's $q\sim\varepsilon$ relation curve, and the numerical size can determine a hardening or softening curve, as shown in Fig. 9.
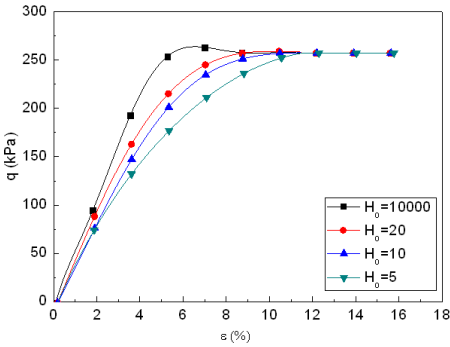

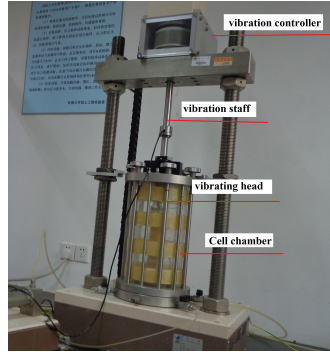Fig. 9. Diagram of H_0 effect on the $q\sim\varepsilon$ relationship

Fig. 10. GDS dynamic triaxial apparatus

4. Experimental study and verification analysis

4.1. Dynamic experimental study

Shield segment and the structure can be affected by moving metro dynamic loads during vibration operation [30, 31]. Studies have shown that the metro dynamic loads produce a vibration waveform that is similar to the sine wave [32]. We performed a GDS dynamic triaxial test on soft soil. As illustrated in Fig. 10, during operation, the vibration staff (controlled by the vibration controller) drives the vibration head oscillating up and down so that vibration loading is applied to the soil in the cell chamber. The location of the soil is in Hexi area of Nanjing, China, Metro line 2 of Nanjing crosses through the area, and the physical and mechanical indexes of soft soil are shown in Table 1 [33].

The samples were prepared as the cylinders that were 38 mm in diameter and 75 mm in height. The effective confining pressure is, respectively, 75 and 150 kPa. We used a half sine wave load; dynamic amplitudes of 10, 15, and 20 N, respectively; and established 10000 vibration times.

Table 1. Physical and mechanical properties of soft clay

w (%)	G_s	I_p	ρ (g/cm³)	e_0
37.3	2.72	17	1.877	0.99

4.2. Comparison and analysis

We selected the confining pressure of $\sigma_d = 75$ kPa, a dynamic amplitude of $F_d = 10$ N, and a vibration frequency $f = 1$ Hz as an example. We then compared calculations results with the test results. The test parameters are as show in Table 2.

Table 2. Parameters of model for clay

E_d/S_u	R_f	m	C_α	M	λ	κ	H_0
3.5	0.72	0.17	0.091	1.42	0.18	0.08	20

As shown in Fig. 11, the test results are compared against the calculation results of the $q\sim\varepsilon_d$ curve. The calculated results by the time-dependent bounding surface model are closer to the experimental value.

As shown in Fig. 12, the calculated results by the time-dependent bounding surface model are closer to the experimental value when compared with the result of strain vs. time curve.
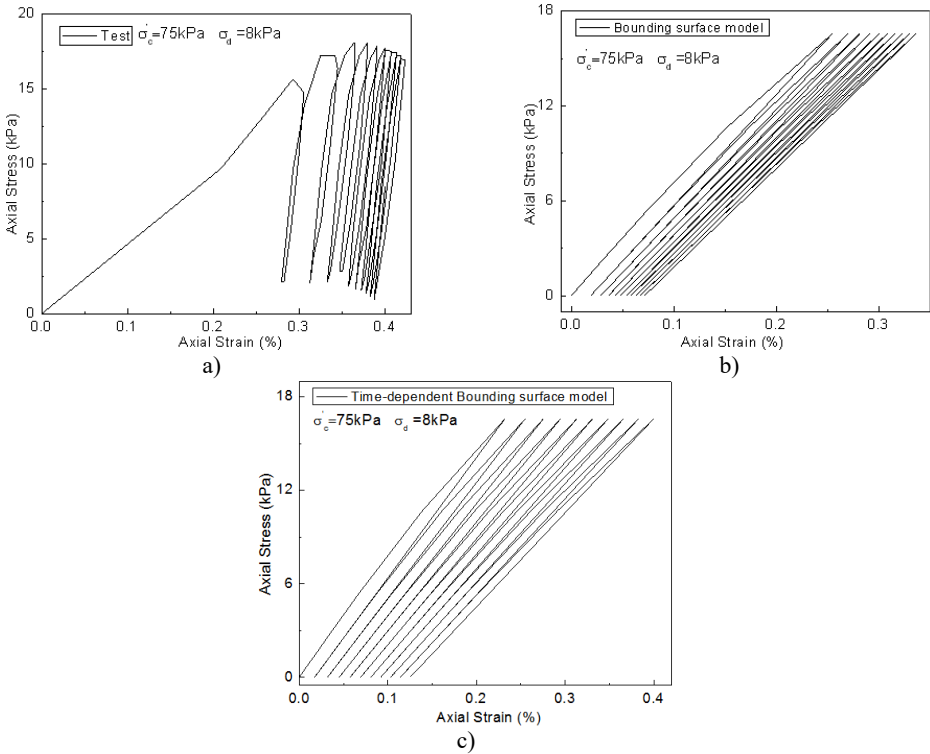
a)

b)

c)

Fig. 11. Comparison between test results and predicted values of the $q \sim \varepsilon_d$ curve
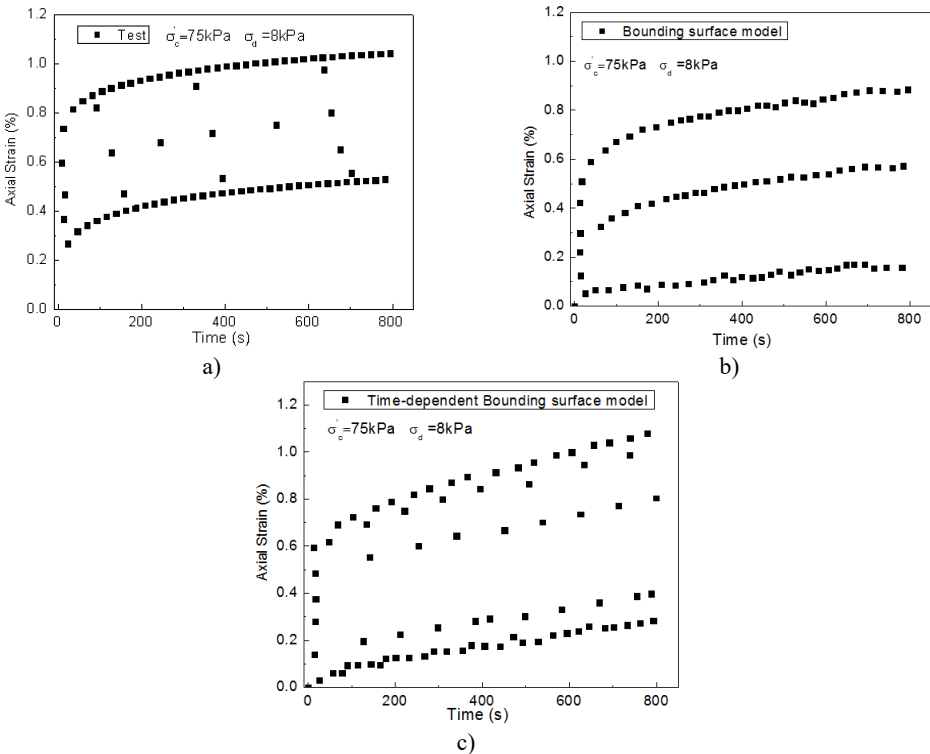

a)

b)

c)

Fig. 12. Comparison between test results and predicted values of the strain vs. time curve

As shown in Fig. 13, the calculated results by the bounding surface model are small when compared with the result of the pore pressure vs. time curve, and the calculated results enter a stable state. The calculated results by the time-dependent bounding surface model is similar to the measured data. Although the turning point is small, it is consistent with the test value as they both increase over time.

Via the above curve comparisons between test results and prediction, we can see that the time-dependent bounding surface model could effectively describe the dynamic characteristics of soft soil under dynamic loads.
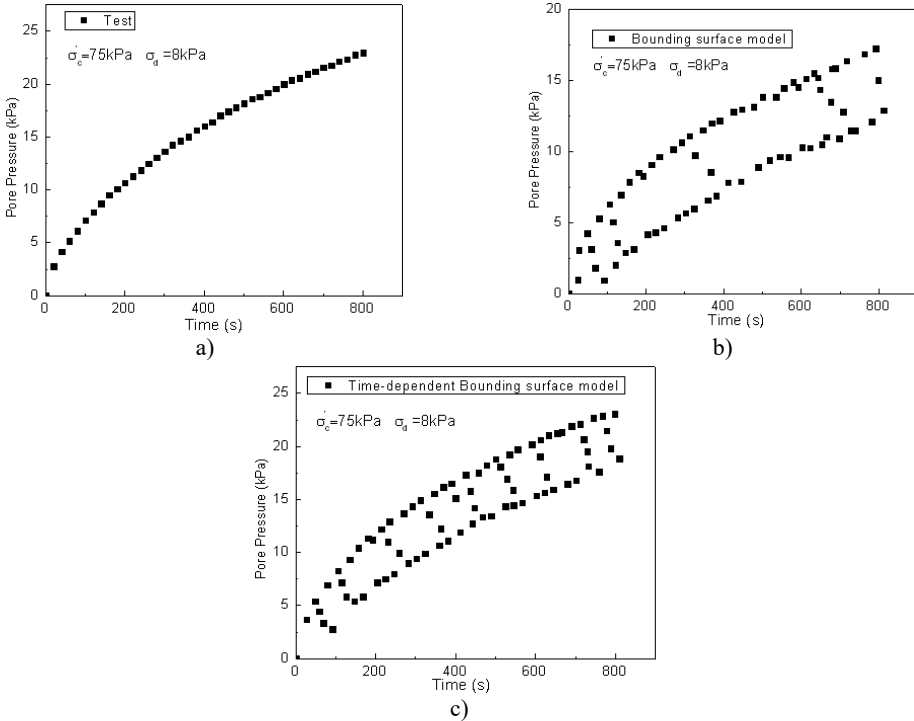

Fig. 13. Comparison between test results and predicted values of the pore pressure vs. time curve

5. Conclusion

This paper studies the dynamic characteristics of soft soil under metro dynamic loads. The conclusions can be drawn from this study:

1. Introducing the Mesri creep model into the boundary surface model allows for the calculation of soil creep under arbitrarily shear stress levels; the shear stress level contains all the stress level statuses (0-100 %). The improved bounding surface model can take into consideration the time effects.

2. The calculation steps have been provided to illustrate the time-dependent bounding surface model using the Newton-Raphson method and carried out secondary development of model.

3. Simulating the dynamic load waveforms had been carried out during GDS dynamic triaxial test for the soft soil, comparing the test results with predicted values. The results showed that the time-dependent bounding surface model more accurately calculated the dynamic strain.

Acknowledgements

References

[1] **Bjerrum L.** Engineering geology of Norwegian normally consolidated marine clays as related to settlements of buildings. 7th Rankine Lecture. Geotechnique, Vol. 17, Issue 2, 1967, p. 83-117.

[2] **Luo J. H., Miao L. C., Wang Z. X., et al.** Modified cam-clay model with dynamic shear modulus under cyclic loads. Journal of Vibroengineering, Vol. 17, 2015, p. 112-124.

[3] **Zhang J. F., Chen J. J., Wang J. H.** Prediction of tunnel displacement induced by adjacent excavation in soft soil. Tunneling and Underground Space Technology, Vol. 36, 2013, p. 24-33.

[4] **Dafalias Y. F., Popov E. P.** A model of non-linearly hardening materials for complex loading. Acta Mechanica, Vol. 21, 1975, p. 173-192.

[5] **Dafalias Y. F., Herrmann L. R.** Bounding surface plasticity. I: Mathematical foundation and hypo-plasticity. Journal of Engineering Mechanics, Vol. 112, Issue 9, 1986, p. 966-987.

[6] **Dafalias Y. F., Herrmann L. R.** Bounding surface plasticity. II: Application to isotropic cohesive soils. Journal of Engineering Mechanics, Vol. 112, Issue 12, 1986, p. 1292-1318.

[7] **Wood D. M.** Soil Behavior and Critical Soil Mechanics. Cambridge University Press, 1990.

[8] **He Z. J., Zhang J. X.** Strength characteristics and failure criterion of plain recycled aggregate concrete under triaxial stress states. Construction and Building Materials, Vol. 54, 2014, p. 354-362.

[9] **Hu C., Liu H. X., Huang W.** Anisotropic bounding-surface plasticity model for the cyclic shakedown and degradation of saturated clay. Computers and Geotechnics, Vol. 44, 2012, p. 34-47.

[10] **Wang Gang, Zhang Jian-Min** Implementation and application of a bounding surface model in MARC. Rock and Soil Mechanics, Vol. 27, Issue 9, 2006, p. 1535-1540, (in Chinese).

[11] **Singh A., Mitchell J. K.** General stress-strain-time function for soils. Journal of Soil Mechanics and Found Engineering Division, American Society of Civil Engineering, Vol. 94, Issue 1, 1968, p. 21-46.

[12] **Kondner R. L.** Hyperbolic stress-strain response: cohesive soils. Journal of Soil Mechanics and Foundations, American Society of Civil Engineering, Vol. 89, Issue 1, 1963, p. 115-143.

[13] **Mesri G., Febres C. E., Shields D. R., Castro A.** Shear-stress-strain-time behavior of clays. Geotechnique, Vol. 31, Issue 4, 1981, p. 537-552.

[14] **Shalabi F. I.** FE analysis of time-dependent behavior of tunneling in squeezing ground using two different creep models. Tunneling and Underground Space Technology, Vol. 20, 2005, p. 271-279.

[15] **Feng S. Y., Wei L. M., He C. Y., He Q.** A computational method for post-construction settlement of high-speed railway bridge pile foundation considering soil creep effect. Journal of Central South University of Technology, Vol. 21, 2014, p. 2921-2927.

[16] **Victor N. K.** Parameter estimation for time-dependent bounding surface models for cohesive soils. Soil Constitutive Models, 2005, p. 237-256.

[17] **Bodas Freitas T. M., David M. P., Lidija Z.** A time dependent constitutive model for soils with isotach viscosity. Computers and Geotechnics, Vol. 38, 2011, p. 809-820.

[18] **Hardin B. O., Black W. L.** Vibration modulus of normally consolidated clay. Journal of the Soil Mechanics and Foundations Division, Vol. 94, Issue 2, 1968, p. 353-369.

[19] **Hardin B. O., Drnevich V. P.** Shear modulus and damping in soils: design equations and curves. Journal of the Soil Mechanics and Foundations Division, Vol. 98, Issue 7, 1972, p. 667-692.

[20] **Taylor D. W.** Fundamentals of Soil Mechanics. Wiley. Literary Licensing, LLC, New York, 1948.

[21] **Papon A., Yin Z.-Y., Riou Y.** Time homogenization for clays subjected to large numbers of cycles. International Journal for Numerical and Analytical Methods in Geomechanics, Vol. 37, Issue 11, 2013, p. 1470-1491.

[22] **Borja R. I., Kavazanjian J. R. E.** A constitutive model for the stress-strain-time behavior of 'wet' clays. Geotechnique, Vol. 35, Issue 3, 1985, p. 283-298.

[23] **Manzari M. T., Nourm A.** On implicit integration of bounding surface plasticity models. Computers and Structures, Vol. 63, Issue 3, 1997, p. 385-395.

[24] **Xu T. H., Zhang L. M.** Numerical implementation of a bounding surface plasticity model for sand under high strain-rate loadings in LS-DYNA. Computers and Geotechnics, Vol. 66, 2015, p. 203-218.

[25] **Manzari M. T., Prachathananukit R.** On integration of cyclic soil plasticity model. Numerical and Analytical Methods in Geomechanics, Vol. 25, Issue 6, 2001, p. 525-549.

[26] **Amorosi A., Boldini D., Germano V.** Implicit integration of a mixed isotropic-kinematic hardening plasticity model for structured clays. International Journal for Numerical and Analytical Methods in Geomechanics, Vol. 32, Issue 10, 2008, p. 1173-1203.

[27] **Mašín D.** Hypoplastic cam-clay model. Geotechnique, Vol. 62, Issue 6, 2012, p. 549-553.
[28] **Subramaniam P., Sunbhadeep Banerjee** Shear modulus degradation model for cohesive soils. Soil Dynamics and Earthquake Engineering, Vol. 53, 2013, p. 210-216.
[29] **Jun Wang, Yuan qiang Cai, Fang Yang** Effects of initial shear stress on cyclic behavior of saturated soft clay. Marine Georesources and Geotechnology, Vol. 31, Issue 1, 2013, p. 86-106.
[30] **Shen Shui-Long, Wu Huai-Na, Cui Yu-Jun** Long-term settlement behaviour of metro tunnels in the soft deposits of Shanghai. Tunneling and Underground Space Technology, Vol. 40, 2014, p. 309-323.
[31] **Ng C. W. W., Liu G. B., Li Q.** Investigation of the long-term tunnel settlement mechanisms of the first metro line in Shanghai. Canadian Geotechnical Journal, Vol. 50, Issue 6, 2013, p. 674-684.
[32] **Zhang Jun-Feng, Chen Jin-Jian, Wang Jian-Hua** Prediction of tunnel displacement induced by adjacent excavation in soft soil. Tunneling and Underground Space Technology, Vol. 36, 2013, p. 24-33.
[33] **Alpan I.** The geotechnical properties of soils. Earth-Science Reviews, Vol. 6, Issue 1, 1970, p. 5-49.

Junhui Luo, Doctoral studies of Southeast University. His current research interests include soil dynamics.
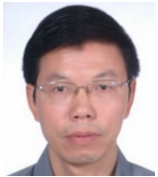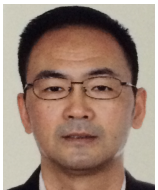

Linchang Miao, Ph.D., Professor of Geotechnical Engineering, Southeast University.

Renjue Li, Undergraduate student of Changzhou Institute of Technology.

Wenbo Shi Doctoral studies of Southeast University. His current research interests include traffic engineering.

Yinan Chen M.S. His current research interests include geotechnical engineering.

Bo Yan received M.S. degree. His current research interests include traffic engineering.